DOI: 10.1002/asia.200800011

A High-Performance Organic Field-Effect Transistor Based on Platinum(II) Porphyrin: Peripheral Substituents on Porphyrin Ligand Significantly Affect Film Structure and Charge Mobility

Chi-Ming Che,*[a] Hai-Feng Xiang,[a, b] Stephen Sin-Yin Chui,[a] Zong-Xiang Xu,[a] V. A. L. Roy,[a] Jessie Jing Yan,[a] Wen-Fu Fu,[c] P. T. Lai,[b] and Ian D. Williams[d]

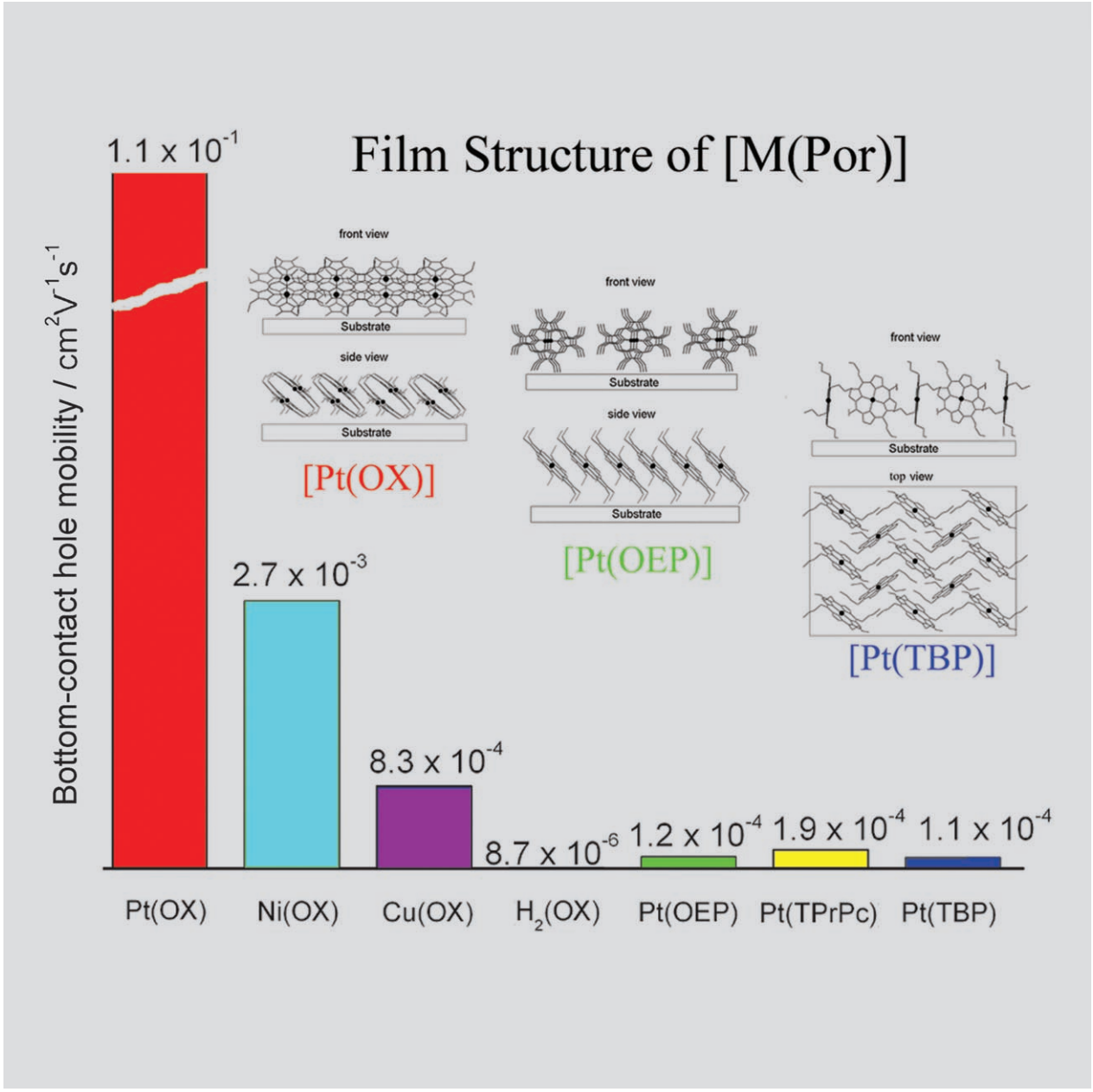

Abstract: Organic field-effect transistors incorporating planar π-conjugated metal-free macrocycles and their metal derivatives are fabricated by vacuum deposition. The crystal structures of [H_2(OX)] (H_2OX = etioporphyrin-I), [Cu(OX)], [Pt(OX)], and [Pt(TBP)] (H_2TBP = *tetra*-(n-butyl)porphyrin) as determined by single crystal X-ray diffraction (XRD), reveal the absence of occluded solvent molecules. The field-effect transistors (FETs) made from thin films of all these metal-free macrocycles and their metal derivatives show a *p*-type semiconductor behavior with a charge mobility (μ) ranging from 10^{-6} to 10^{-1} $cm^2V^{-1}s^{-1}$. Annealing the as-deposited Pt(OX) film leads to the formation of a polycrystalline film that exhibits excellent overall charge transport properties with a charge mobility of up to 3.2×10^{-1} $cm^2V^{-1}s^{-1}$, which is the best value reported for a metalloporphyrin. Compared with their metal derivatives, the field-effect transistors made from thin films of metal-free macrocycles (except *tetra*-(*n*-propyl)porphycene) have significantly lower μ values (3.0×10^{-6}–3.7×10^{-5} $cm^2V^{-1}s^{-1}$).

Keywords: macrocyclic ligands · materials science · molecular electronics · OFET (organic field-effect transistor) · X-ray diffraction

Introduction

Interest in organic thin-film transistors (OTFTs) has grown dramatically over recent years because of their potential practical applications in active-matrix backplanes for flexible displays, sensors, and memory devices.[1] In this regard, there has been a considerable interest in the design and synthesis of planar π-conjugated molecules such as pentacene,[2] oligothiophene,[3] arylacetylene,[4] indolo-[3,2-*b*]-carbazole,[5] tetrathiafulvalene,[6] and perylene,[7] for uses in OTFT fabrication. The intermolecular arrangements of these organic molecules, in each case, are dominated by π···π stacking interactions, leading to the formation of highly oriented polycrystalline films with good charge transport properties. Recently, transition-metal complexes have been demonstrated to be an alternative source of new materials for the development of organic field-effect transistors.[8] A notable example is copper(II) phthalocyanine abbreviated as Cu(Pc), which has been extensively used in OTFT fabrication, for which a maximum hole charge mobility of 10^{-2} $cm^2V^{-1}s^{-1}$ has been achieved.[8a] Noro et al. recently reported the construction of a field-effect transistor made from a nickel(II) complex with a *o*-diiminobenzosemiquinonate ligand, which has a comparable charge mobility of 3.8×10^{-2} $cm^2V^{-1}s^{-1}$.[8e] In the literature, there are few studies on field-effect transistors made from porphyrins,[9] metalloporphyrins, and related derivatives,[10] despite the fact that these π-conjugated compounds and metal complexes have a variety of applications such as in organic light-emitting diodes (OLEDs),[11] as luminescent oxygen sensors,[12] as phosphorescent probes,[13] and in photovoltaic cells.[14] Porphyrins and metalloporphyrins are robust, easily prepared, and have varying electronic structures and interesting excited-state properties.[15] The reported field-effect transistors made from thin film of 5,10,15,20-tetra-(phenyl)porphyrin[9a] and platinum(II) 2,3,7,8,12,13,17,18-octaethyl-21*H*,23*H*-porphyrin Pt(OEP)[10b] exhibited a moderate charge mobility of 7.0×10^{-3} $cm^2V^{-1}s^{-1}$ and 2.2×10^{-4} $cm^2V^{-1}s^{-1}$, respectively. However, when Pt(OEP) film was used as a phosphorescent dopant for a red light OLED, a low charge mobility of 10^{-5} $cm^2V^{-1}s^{-1}$ was observed.[11,14a] Herein, we described a series of field-effect transistors made from thin films of metal-free porphyrins and related macrocyclic compounds: etioporphyrin-I [H_2(OX)], 2,3,7,8,12,13,17,18-octaethyl-21*H*,23*H*-porphine [H_2(OEP)], phthalocyanine [H_2(Pc)], 2,7,12,17-tetra-(*n*-propyl)-porphycene [H_2(TPrPc)], and 5,10,15,20-*tetra*-(n-butyl)-porphyrin [H_2(TBP)], as well as their metal(II) derivatives (Pt, Ni, and Cu) (Scheme 1). We

[a] Prof. C.-M. Che, Dr. H.-F. Xiang, Dr. S. S.-Y. Chui, Z.-X. Xu, Dr. V. A. L. Roy, J. J. Yan
Department of Chemistry and HKU-CAS
Joint laboratory on New Materials
The University of Hong Kong
Pokfulam Road, HKSAR (China)
Fax: (+852) 2857-1586
E-mail: cmche@hku.hk

[b] Dr. H.-F. Xiang, Prof. P. T. Lai
Department of Electrical & Electronic Engineering
The University of Hong Kong
Pokfulam Road, HKSAR (China)

[c] Prof. W.-F. Fu
Technical Institute of Physics and Chemistry
The Chinese Academy of Science
Beijing, 100080 (China)

[d] Prof. I. D. Williams
Department of Chemistry
The Hong Kong University of Science and Technology
Clear Water Bay, Kowloon, HKSAR (China)

Supporting information for this article is available on the WWW under http://dx.doi.org/10.1002/asia.200800011.

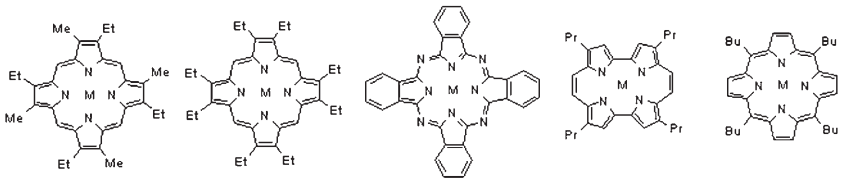

Scheme 1. Structures of the metal-free porphyrins and their metal derivatives.

also describe their charge transport properties following annealing treatment of the as-deposited thin films at 60–120 °C. Using single crystal X-ray structures and grazing incidence X-ray diffraction data, we have examined the effects of peripheral substituents on porphyrin ligands and complexed metal ions on the film structure and charge mobility of the as-fabricated field-effect transistors. A high-performance top-contact field-effect transistor made from an annealed Pt(OX) film exhibited a charge mobility of up to 3.2×10^{-1} $cm^2V^{-1}s^{-1}$, which is the best value for metalloporphyrin materials reported in the literature. Both packing of molecules and film morphology (continuity and crystal grain) are important parameters in determining the overall charge transport properties of organic field-effect transistors.

Results and Discussion

Detailed procedures for the synthesis of H_2(TBP) and H_2(TPrPc), as well as for metalloporphyrins M(OX), M(OEP) (M = Pt, Ni, Cu), Pt(Pc), Pt(TBP), and Pt(TPrPc) studied in this work are given in the Supporting Information. The isolated yields of all the metal complexes were 70~80%. The preparation of single crystals of H_2(OX), Cu(OX), Pt(OX) suitable for X-ray crystal structure determination proved to be a difficult task, as either a fine powder sample or twinned crystals were frequently encountered. We found that slow evaporation of $CHCl_3/CH_2Cl_2$ solutions of these compounds or metal complexes gave tiny air-stable crystals (with a maximum dimension $<200\,\mu m$), from which fine-needle [H_2(OX) and Cu(OX)] or thin-plate Pt(OX) crystal habit was observed. To establish the arrangement of molecules in the as-deposited and annealed polycrystalline films of Pt(OX), Cu(OX), H_2(OX), and Pt(TBP), only the data from the X-ray crystal structures that did not contain occluded solvent molecules were used. In this regard, the data from the previously reported X-ray crystal structures of M(OEP) (M = Pt, Ni, Cu, and H_2),[16–19] M(Pc) (M = Pt, Cu, and H_2),[20] H_2(TBP),[21] and M(TPrPc) (M = Pt, H_2)[22c,d] were used.

X-ray Crystal Structures

The crystal data of Pt(OX), Cu(OX), H_2(OX), and Pt(TBP), and selected bond distances/angles are listed in the Supporting Information, Tables S1 and S2. Figure 1 depicts the molecular structure of Pt(OX) and the packing of Pt(OX) molecules. The Pt atom is roughly coplanar with the mean plane of the porphyrin macrocycle. Owing to the presence of mirror and rotation symmetries, each asymmetric unit contains one-eighth of the Pt(OX) molecule, and the Pt atom lies on a special position ($^1/_2$,$^1/_4$,$^1/_8$). All four pyrrole-ring moieties of each Pt(OX) molecule simultaneously have intermolecular π···π interactions (3.409 Å) with its neighbors along the three crystallographic directions. This results in a π-stacked molecular arrangement that enables a close packing in the X-ray crystal structure. The Pt(OX) molecules crystallized in a tetragonal space group of $I4_1/amd$ (No. 141) that is isomorphic to Ni(OX).[23] The Pt–N distances of 1.94(1) Å are shorter than those of Ni–N distances found in Ni(OX) (1.957 Å) and Pt(OEP) (2.012 Å).[16] Because of the lattice symmetry imposed on Pt(OX), the methyl and ethyl substituents were regarded as statistically disordered moieties. There are no direct metal···metal interactions, as revealed by the shortest non bonded Pt···Pt contacts of 7.952(1) Å.

Similar columnar-like π-stacked arrangements of Cu(OX) or H_2(OX) molecules with weak π···π interactions (3.500–3.532 Å for Cu(OX) and 3.485–3.583 Å for H_2(OX)) have been found in their respective X-ray crystal structures (Supporting Information, Figures S1 and S2). Each columnar stack of Cu(OX) molecules is laterally segregated and extends along one direction of the X-ray crystal structure. There are non bonded Cu···C distances of 3.42 Å, as found in the X-ray crystal structure of Cu(OX). The Cu atom is coplanar with the mean plane of porphyrin macrocycle and the Cu atom lies on the inversion center so that half of the molecule is contained per asymmetric unit. The Cu–N distances of 1.988(5) Å and 2.018(4) Å are slightly longer than those of 1.944 Å and 1.997 Å for Cu(OEP).[18] A non centrosymmetric arrangement is noted for H_2(OX), and the four methyl carbons of the ethyl substituents are displaced by approximately 1 Å above or below the mean plane of the porphyrin macrocycle. Such an arrangement results in a slightly curved molecular conformation with the dihedral angles, between the two mean planes of adjacent pyrrole rings of the molecule, being 1.2–7.4° (Supporting Information Table S2).

Abstract in Chinese:

本文以平面型的π-共轭卟啉化合物及其金属衍生物为活性层利用高真空蒸镀的方法制备了有机场效应晶体管。采用单晶 X-射线衍射法研究相关卟啉化合物（[H_2(OX)] (H_2OX = etioporphyrin-I), [Cu(OX)], [Pt(OX)] 和 [Pt(TBP)] (H_2TBP = *tetra*-(*n*-butyl)porphyrin)）的晶体结构，研究其π-π 共轭体系的差别及其在薄膜中分子排列的不同对场效应晶体管器件影响。研究发现该系列卟啉化合物及其金属衍生物主要表现为 p-型半导体性质，其金属衍生物的空穴迁移率为 10^{-6} ~ 10^{-1} $cm^2V^{-1}s^{-1}$，要远高于相应的卟啉化合物(3.0×10^{-6}–3.7×10^{-5} $cm^2V^{-1}s^{-1}$)，而且经过退热处理可以提高晶体管器件性能，其中的[Pt(OX)]具有最高的空穴迁移率，经过退热处理后，从 1.1×10^{-2} $cm^2V^{-1}s^{-1}$ 增加到 3.2×10^{-1} $cm^2V^{-1}s^{-1}$，是已报道金属卟啉化合物中最高的

CHEMISTRY
AN ASIAN JOURNAL

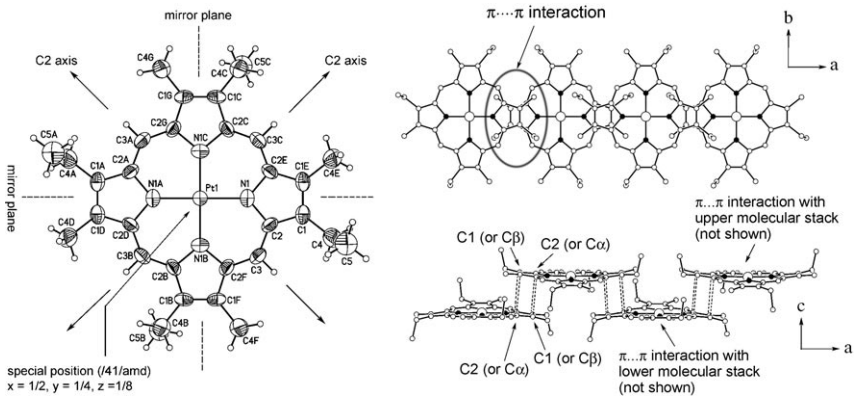

Figure 1. ORTEP drawing (30% probability ellipsoids) of Pt(OX). Owing to the mirror and rotation symmetry of the crystal lattice, the four CH_3 moieties (C5, C5A, C5B, and C5C) of the ethyl substituents are statistically disordered (left). Perspective views of the packing of Pt(OX) molecules, showing that the weak π···π stacking interactions (3.409 Å) (dotted lines) extending along three principle crystallographic directions effectively enables a close molecular packing (right).

Figure 2 shows a perspective view of the packing of Pt(TBP) molecules in a herringbone-like arrangement. The axial sites of each Pt atom interact weakly with two neighboring pyrrolic C–H hydrogen atoms [Pt1 (x, *y*, *z*) ··H3′–C3′ (x, $^1/_2-$y, $^1/_2+$z) and Pt1 (x, *y*, *z*)···H″–C″ (−x, $^1/_2+$y, $-^1/_2-$z)] with a non bonded Pt···H distance of 2.871 Å and a Pt···H–C angle of 168.2°. This type of weak interaction may be classified as a non agostic C–H···M interaction.[24] Neighboring Pt(TBP) molecules are roughly orthogonal to each other. The shortest centroid-to-centroid distance between adjacent Pt(TBP) molecules is 7.918(1) Å, precluding any Pt···Pt interactions. The Pt–N distances of 2.024(3) Å and 2.027(3) Å are comparable to that of the other platinum(II) *meso*-substituted porphyrins.[25] In the literature, a similar herringbone-like packing of molecules has previously been reported in the X-ray crystal structure of H_2(TBP).[21] The X-ray crystal structures of Pt(TBP) and H_2TBP reveal no intermolecular π···π interactions because the shortest non bonded neighboring C···C distances are greater than 4.0 Å in each case. Compared with the reported X-ray crystal structures of Pt(TPP)[25a] and Pt(F_{28}TPP)[25d] (H_2TPP = *meso*-tetraphenylporphyrin and H_2F_{28}TPP = perfluorinated *meso*-tetraphenylporphyrin), Pt(TBP) adopts a less ruffled conformation, as evidenced by the small dihedral angles (0.1–1.2°) between the two mean planes of adjacent pyrrole rings of the molecule (Supporting Information, Table S2).

PXRD and GIXRD Patterns

The crystalline-phase purity of the as-synthesized and purchased organic compounds and metal complexes studied in this work were verified by powder X-ray diffraction (PXRD). The experimental PXRD patterns of Pt(OX), Cu(OX), H_2(OX), and Pt(TBP) generally match the corresponding simulated PXRD patterns using the data of single crystal X-ray structures (Supporting Information Figure S3). There are small variations in the relative peak intensities attributed to an effect of preferred orientation caused by the crystallite-shape anisotropy.

Figure 3 shows the grazing incidence X-ray diffraction (GIXRD) pattern of the Pt(OX) film before and after the annealing treatment at 60 °C and 80 °C, as well as a proposed orientation of the molecules in the thin film annealed at 80 °C. Prior to the annealing treatment, there are two diffraction peaks with 2θ values at 7.47° and 8.25°, indicating that two molecular orientations with *d* spacing values of 11.85 Å and 10.74 Å, respectively, were present. When the as-deposited Pt(OX) film was annealed at 60 °C, the ratio of the area of these two peaks changed from 60:40 to 53:47.

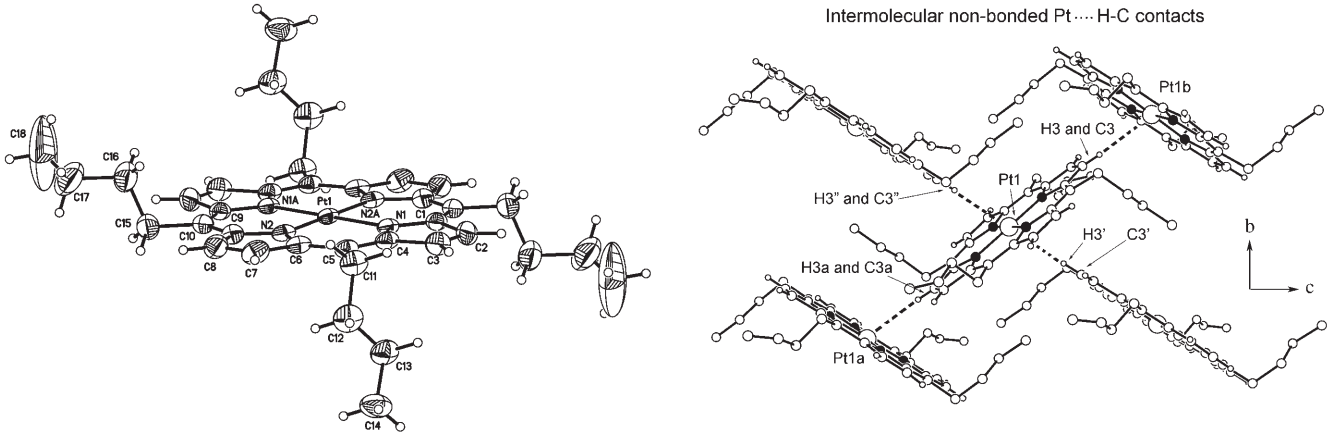

Figure 2. ORTEP drawing (30% probability) of Pt(TBP) (left). Perspective view of a 'herringbone-like' arrangement of Pt(TBP) molecules with weak Pt···H–C interactions (e. g. Pt1···H3′ distance = 2.871 Å, dotted lines and Pt1···H3′–C3′ angle = 168.2°, symmetry code: x, *y*, *z* for Pt1, H3 and C3; −x, −*y*, −*z* for H3a and C3a; x, $^1/_2-$*y*, $^1/_2+$*z* for H3′ and C3′; −*x*, $^1/_2+$*y*, $-^1/_2-$*z* for H″ and C3″) (right).

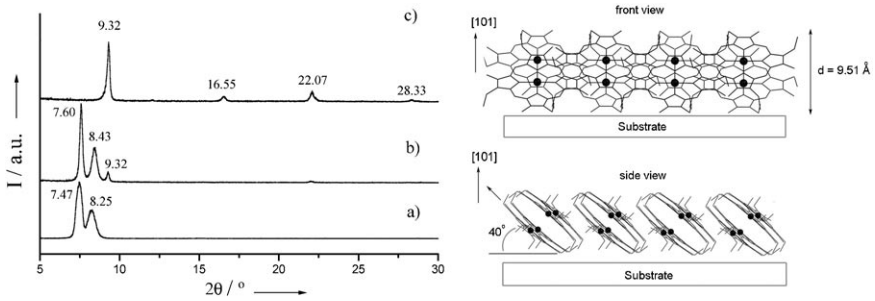

Figure 3. GIXRD patterns of the as-deposited Pt(OX) film before (a) and after annealing treatment at 60 °C (b) and at 80 °C (c). The numerical values indicate the peak positions (°) in the 2θ scale (left). The front and side views of a proposed packing of Pt(OX) molecules in the thin film being annealed at 80 °C. The Pt(OX) molecules are coherently oriented along the [101] Miller plane of the X-ray crystal structure at an angle of 40° with the plane of the substrate (right).

The two peak positions were slightly right-shifted, and an additional weak peak at 9.32° appeared. When this thin film was further annealed at 80 °C, the diffraction peaks at 7.60° and 8.43° completely disappeared, whereas the intensity of the diffraction peak at 9.32° dramatically increased, and three additional high-order diffraction peaks with 2θ values at 16.55°, 22.07°, and 28.33° developed. These four diffraction peaks match the calculated positions of 9.36°, 16.71°, 22.43°, and 28.34° for the respective [101], [112], [103], and [303] Miller planes of the X-ray crystal structure of Pt(OX). As the diffraction peak at 9.32° is the strongest, and is close to the calculated position (9.36°) of the [101] Miller plane, the Pt(OX) molecules in the thin film annealed at 80 °C are coherently aligned, and the mean plane of each Pt(OX) molecule forms an angle of approximately 40° with the plane of the substrate.

A similar π-stacked arrangement of metalloporphyrin molecules has also been found in the Ni(OX) film that was annealed at 140–160 °C (Supporting Information, Figure S4). However, the π-stacked molecular arrangement was minor as most of Ni(OX) molecules were packed with a lamellar *d* spacing value of 12.30 Å, as shown by the strong diffraction peak with a 2θ value of 7.20°. Subjecting the as-deposited Cu(OX) film to the same annealing treatment at 60–160 °C did not induce any structural transition, and the position of the two diffraction peaks (2θ = 7.43° and 8.65°) remained unaltered, whereas the peak intensities decreased with annealing temperature. In the case of H_2(OX), there were two diffraction peaks with 2θ values of 6.73° and 9.09° in the as-deposited film (Supporting Information, Figure S5). After the annealing treatment at 100 °C, the peak at 6.73° disappeared and the intensity of the peak at 9.09° increased with a small right-shift of 0.13°. As the peak at 9.09° is close to the calculated position (9.135°) of the [010] Miller plane of the X-ray crystal structure of H_2(OX), it suggests that the H_2(OX) molecules were aligned in a columnar π-stacked arrangement, in which the [010] Miller plane was parallel to the plane of the substrate. When the H_2(OX) film was further annealed at 140 °C, the diffraction peak at 9.09° broadened.

The peripheral substituents on the porphyrin macrocycle significantly affects the packing of molecules in the thin film prepared by a deposition method. Figure 4 shows the GIXRD patterns of the as-deposited M(OEP) films (M = Pt, Ni Cu, and H_2) as well as a proposed packing of molecules in the as-deposited films. The GIXRD pattern for the as-deposited M(OEP) films (M = Pt, Ni Cu, and H_2) individually displayed a single diffraction peak with 2θ value near 7.98°, that matched the calculated peak positions (7.930° and 7.928°) of the [1$\bar{1}$0] Miller plane of the X-ray crystal structures of Ni(OEP) and Cu(OEP),[17,18] but significantly deviated from that of 8.891° for the [001] Miller plane, and that of 8.312° for the [010] Miller plane of the X-ray crystal structures of Pt(OEP)[16] and H_2(OEP),[19] respectively. Based on this finding, a columnar π-stacked arrangement of M(OEP) molecules (M = Pt, Ni, Cu, H_2) is expected in these as-deposited films, and these π-stacked M(OEP) molecules were oriented at an angle of approximately 55° from the plane of the substrate. When these thin films were annealed at 140 °C, both the peak position and intensity of the single diffraction peak at 7.98° showed little change.

Figure 5 shows the GIXRD pattern of the as-deposited Pt(TBP) and H_2(TBP) films and a proposed packing arrangement of Pt(TBP) molecules in the as-deposited film. The as-deposited Pt(TBP) film was well-ordered with high crystallinity. The Pt(TBP) molecules are proposed to stand on the substrate because the two observed diffraction peaks

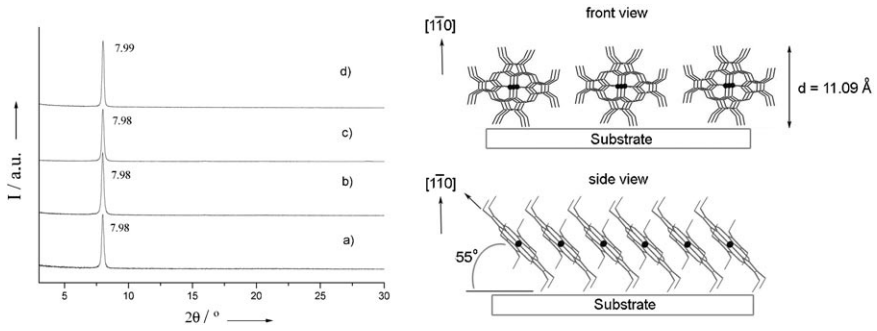

Figure 4. GIXRD patterns of the as-deposited M(OEP) films M = Pt (a), Ni (b), Cu (c), and H_2 (d). The numbers indicate the peak positions (°) in the 2θ scale (left). The front and side views of a proposed packing of M(OEP) molecules (M = Pt, Ni, Cu, or H_2) in the as-deposited films oriented along the [1$\bar{1}$0] Miller plane of the X-ray crystal structure of Cu(OEP) at an angle of 55° with the plane of the substrate (right).

CHEMISTRY
AN ASIAN JOURNAL

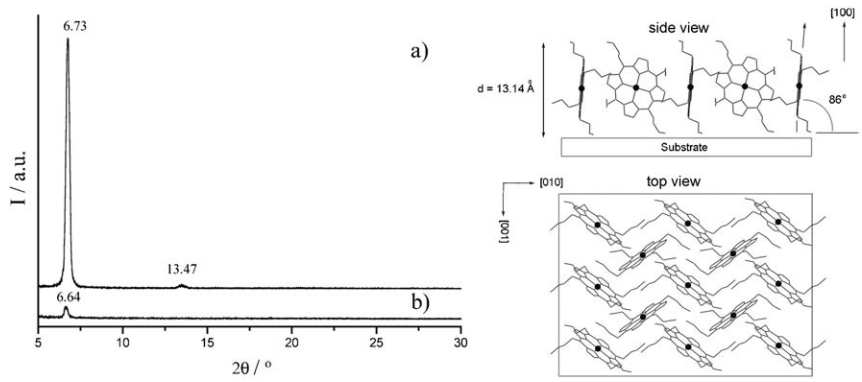

Figure 5. GIXRD patterns of the as-deposited (a) Pt(TBP) and (b) H_2(TBP) films. The numbers indicate the peak positions (°) in the 2θ scale (left). The side and top views of a proposed packing of Pt(TBP) molecules in the as-deposited film oriented along the [100] Miller plane of the X-ray crystal structure of Pt(TBP) at an angle of 86° with the plane of the substrate. Note that the Pt(TBP) molecules are nearly orthogonal to each other, and to the substrate (right).

with 2θ values at 6.73° and 13.47° match the respective calculated positions of 6.743° and 13.510° for the [100] and [200] Miller planes of the X-ray crystal structure of Pt(TBP), respectively. The mean plane of each Pt(TBP) macrocycle is almost orthogonal to its neighbors, leading to a herringbone-like arrangement of Pt(TBP) molecules on the substrate. Furthermore, the as-deposited H_2(TBP) film adopted a similar molecular packing as that observed for the Pt(TBP) film, but the packing was less ordered as evidenced by the presence of a weaker diffraction peak with a 2θ value near 6.64°. Subjecting the as-deposited Pt(TBP) and H_2(TBP) films to an annealing treatment at 60–160 °C did not induce any structural transition.

Further studies using GIXRD revealed that the M(Pc) (M = Pt, Cu, and H_2) molecules adopted a similar π-stacked columnar arrangement in the as-deposited M(Pc) films (Supporting Information, Figure S6). The 2θ values of the single diffraction peak near 6.78–6.90° in each case, were close to that (6.74–6.87°) of the [200] Miller plane of the X-ray crystal structures of α- and γ- polymorphic forms of Pt(Pc),[20b] and comparable to that of 7.011° for the [100] Miller plane, and 7.023° for the [001] Miller plane of the X-ray crystal structures of the β-form of Cu(Pc)[20a] and H_2(Pc),[20c] respectively. In the case of Pt(TPrPc) (Supporting Information, Figure S7), the 2θ values of 6.94° and 9.12° of the two diffraction peaks were close to that (7.01° and 9.13°) of the respective [001] and [010] Miller planes of the X-ray crystal structure of Pt(TPrPc).[22d] The H_2(TPrPc) film was less crystalline and the 2θ value of the weak diffraction peak near 6.90° matched the calculated peak position of 6.94° of the [002] Miller plane of the X-ray crystal structure of H_2(TPrPc).[22c]

Charge Mobility of the Field-Effect Transistors

All the π-conjugated macrocyclic compounds and their metal derivatives exhibited a moderate thermal stability with onset decomposition temperatures at around 120–350 °C under an N_2 atmosphere. The TGA curves of these compounds and their metal derivatives are given in the Supporting Information, Figure S8. All the metal-free porphyrins decomposed at temperatures above 400–650 °C, whereas the metal derivatives exhibited a weight loss of 70–85 % in the temperature range of 300–500 °C, forming black residues containing either Pt-metal particles (for the Pt-containing derivatives) or metal oxides (CuO/NiO for the Cu/Ni-containing derivatives). The performance of field-effect transistors made from thin films of H_2(OX) and its metal derivatives are summarized in Table 1. Even without an annealing treatment, the top-contact field-effect transistor made from the Pt(OX) film showed a significantly higher charge mobility (μ) of $1.1\times$

Table 1. Device performance of the field-effect transistors made from the as-deposited and annealed films of H_2(OX) and its metal(II) derivatives.

Entry	Onset decomposition temperature [°C]	Device geometry	Annealing temperature [°C]	Charge mobility [$cm^2V^{-1}s^{-1}$]	Threshold voltage [V]	On/off Ratio
Pt(OX)	300	Bottom contact	25	3.7×10^{-5}	−7	10^3
			60	6.1×10^{-5}	−4	10^3
			80	1.1×10^{-1}	−9	10^3
			100	3.9×10^{-2}	−10	10^4
			120	3.0×10^{-2}	−17	10^4
		Top contact	25	1.1×10^{-2}	−29	10^1
			60	1.9×10^{-1}	−16	10^3
			80	3.2×10^{-1}	−9	10^3
			120	1.0×10^{-1}	−4	10^2
Cu(OX)	300	Bottom contact	25	1.4×10^{-4}	−1	10^1
			60	2.1×10^{-4}	4	10^3
			80	8.3×10^{-4}	−10	10^4
			100	5.5×10^{-4}	−21	10^3
			120	4.3×10^{-4}	−11	10^4
Ni(OX)	300	Bottom contact	25	1.1×10^{-3}	3	10^3
			80	2.7×10^{-3}	7	10^2
			100	2.0×10^{-3}	−2.3	10^3
			120	1.7×10^{-3}	−3.4	10^3
			140	1.4×10^{-3}	−6.7	10^3
			160	5.6×10^{-5}	−13	10^2
H_2(OX)	300	Bottom contact	25	8.7×10^{-6}	−27	10^1
			80	–	–	–

$10^{-2}\,cm^2V^{-1}s^{-1}$ than that of $3.7\times10^{-5}\,cm^2V^{-1}s^{-1}$ for the bottom-contact transistor. Figure 6 shows the output and transfer characteristics of the top- and bottom-contact field-effect transistors made from the Pt(OX) film that was annealed at 80 °C. There was an increase in channel current for increasing negative gate voltages, indicative of atypical *p*-channel FET behavior with saturating drain current at high source-drain voltages. For the top- and bottom-contact field-effect transistors made from a Pt(OX) film, the charge mobility extracted from the saturation regime of the output curves are $3.2\times10^{-1}\,cm^2V^{-1}s^{-1}$ and $1.1\times10^{-1}\,cm^2V^{-1}s^{-1}$, respectively. The top-contact field-effect transistor made from the annealed Pt(OX) film was analyzed using transient measurements of the drain current, keeping the drain-source and gate voltage constant at −40 V (Supporting Information, Figure S9). The drain current decayed exponentially and took several minutes to reach background level or to completely suppress the current in the channel. This decay was reproducible as long as the transistor was kept unbiased in an N_2 glove box. The devices made from annealed Pt(OX) films showed a considerably high stability and the overall device performances did not change over a period of six months.

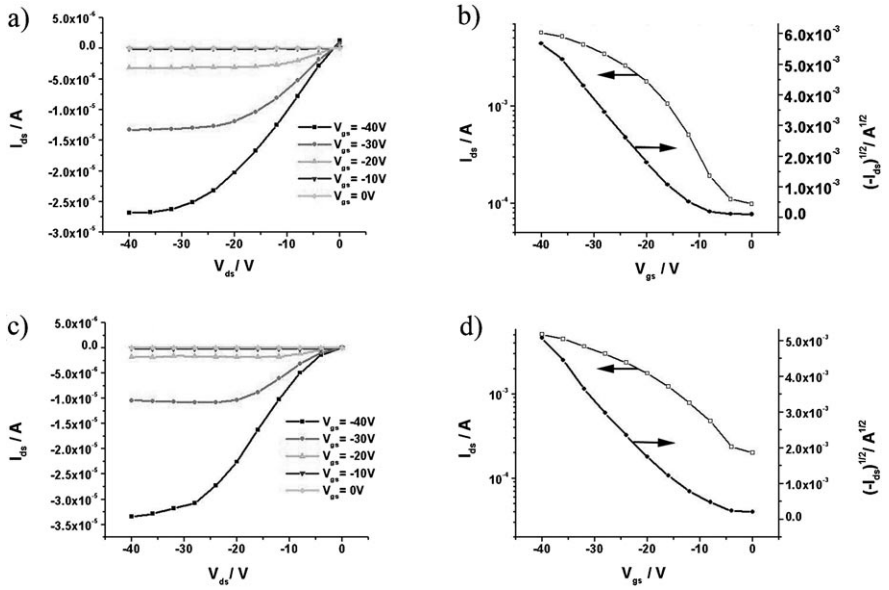

Figure 6. Output (left) and transfer (right) characteristics of the top-contact (channel length 30 μm, channel width 250 μm, (a) and (b), and the bottom-contact (channel length 100 μm, channel width 3000 μm, (c) and (d) transistors made from the Pt(OX) film annealed at 80 °C.

Device performance of the field-effect transistors made from thin films of M(OEP) (M = Pt, Cu, Ni, H_2), M(Pc) (M = Pt, Cu, H_2), M(TPrPc), and M(TBP) (M = Pt, H_2), are given in the Supporting Information, Table S3). All of them consistently exhibited a *p*-channel FET behavior. Without an annealing treatment, the field-effect charge mobility was found to vary over a wide range of 10^{-3}–$10^{-6}\,cm^2V^{-1}s^{-1}$. The field-effect transistors made from Ni(OX) and Cu(OX) films had a low optimal charge mobility of 10^{-3} and $10^{-4}\,cm^2V^{-1}s^{-1}$, respectively. For the Pt(OEP), Pt(TBP), and Pt(TPrPc) films, the charge mobility was in the range of 10^{-4} to $10^{-5}\,cm^2V^{-1}s^{-1}$. Even with an annealing treatment at 80 °C, the H_2(TBP), H_2(OX), H_2(OEP), Pt(Pc), and Pt(TPrPc) films showed no transistor performance. Upon annealing up to 120 °C, the increase in charge mobility of other macrocycles and their metal derivatives was modest, for example, Ni(OX) (×2.5 times); Cu(OX) (×6 times); Ni(OEP) (×38 times); Cu(OEP) (×5 times); Pt(OEP) (×7.5 times); Cu(Pc) (×2.5 times); H_2(Pc) (×1.5 times); H_2(TPrPc) (×1.5 times); and Pt(TBP) (×1.5 times). However, a decrease of 1.5–2.5-fold of the charge mobility of the annealed Cu(Pc), H_2(Pc), Pt(TBP), and H_2(TPrPc) films was observed. The charge mobility of the as-deposited Pt(Pc) film was lower than those of the as-deposited Cu(Pc) and H_2(Pc) films, even though the packing of molecules in these three films were similar, with an identical *d* spacing value of 12.8 Å.

Film Morphological Studies Using SEM

Besides molecular packing, the peripheral substituents on Pt^{II} porphyrins were found to affect the morphology of the as-deposited and annealed films, which consequently altered the charge mobility of as-fabricated field-effect transistors. Figure 7 shows the scanning electron microscopy (SEM) images of a polycrystalline Pt(OX) film deposited on a SiO_2/Si substrate, before and after annealing treatment at 80 °C and 120 °C.

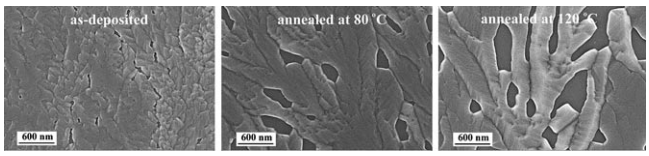

Figure 7. SEM images of the top views of the as-deposited Pt(OX) film before (left) and after annealing treatments at 80 °C (middle) and 120 °C (right).

The as-deposited Pt(OX) film was relatively smooth and almost covered by plate-like crystallite grains sized between 50–100 nm. When this film was annealed at 80 °C, the crystallite grains fused together, resulting in the formation of crack defects covering approximately 6% of the image area.

At 120 °C, the percentage of crack defects increased to about 18%, which could account for the drop in charge mobility from 1.1×10^{-1} to 3.0×10^{-2} $cm^2V^{-1}s^{-1}$ of the bottom-contact Pt(OX) device. These crack defects may be attributed to a mismatch in thermal expansion coefficients between the Pt(OX) film and SiO_2/Si substrate.[26] In contrast, the as-deposited Ni(OX), Cu(OX), and H_2(OX) films were fairly continuous, and the percentage of crack defects increased with annealing temperature (Supporting Information, Figure S10). It is noteworthy that rod-shaped crystallites were obtained when the Ni(OX) and Cu(OX) films were annealed at 80 °C and 120 °C, respectively. The reason for the formation of such rod-like crystallites is not clear, and a probable cause may be related to recrystallization of the hot films upon cooling to room temperature. Crystallite grain boundaries were formed as a result of the air gaps in the annealed Ni(OX) and Cu(OX) films, and these grain boundaries likely led to a 50% drop in the charge mobility [Ni(OX): 2.7×10^{-3} (80 °C)→1.7×10^{-3} (120 °C); Cu(OX): 8.3×10^{-4} (80 °C)→4.3×10^{-4} (120 °C)]. A discontinuous and cracked film was formed when the H_2(OX) film was annealed at 120 °C, leading to a low charge mobility.

The SEM images of the as-deposited and annealed films made from Pt(OEP), Pt(Pc), Pt(TBP), and Pt(TPrPc) were recorded and are provided in the Supporting Information, Figure S11. With the exception of the Pt(TPrPc) film, all the as-deposited Pt^{II} films were uniformly covered with crystallite grains of variable shapes/sizes. For instance, the Pt(OEP) film contained needle-like crystallite grains (1000–2000 nm long, 30–50 nm wide), whereas granular-shaped particles with average diameter of approximately 25–40 nm and 100–140 nm were found for the Pt(Pc) and Pt(TBP) films, respectively. The difference in the charge mobilities of field-effect transistors made from the as-deposited Pt(OEP), Pt(Pc), and Pt(TBP) films did not appear to correlate with the film morphology, as all the polycrystalline films were similarly covered with crystallite grains with a low percentage of insulating grain boundaries. Unlike the Pt(OX) film, annealing the as-deposited Pt(OEP), Pt(Pc), and Pt(TBP) films at 80 °C or 120 °C did not induce any morphological change. We found that there was a considerable number of air gaps between neighboring crystallites in the Pt(TPrPc) film (Supporting Information, Figure S11d), which accounts for its low charge mobility of 10^{-5} $cm^2V^{-1}s^{-1}$. A higher charge mobility of 10^{-4} $cm^2V^{-1}s^{-1}$ was observed for the as-deposited H_2(TPrPc) film fabricated under the same deposition conditions. This may be attributed to the difference in film morphology, as the H_2(TPrPc) film was completely covered with crystallite grains (Supporting Information, Figure S12).

Discussion

Although porphyrins, metalloporphyrins, and related macrocycles have been extensively studied over the past decades, their utilization for fabrication of field-effect transistors has received less attention. Pt(OEP)-based transistor-driven electronic devices, such as OLEDs and photovoltaic cells have been reported to have a low charge mobility (~10^{-5} $cm^2V^{-1}s^{-1}$).[11,14] In this work, a slight variation in the peripheral substituents, that is from H_2(OEP) to H_2(OX), can significantly alter the arrangement of Pt(Por) molecules (H_2(Por) = H_2OEP and H_2OX) in the as-deposited crystalline film, consequently leading to a dramatic increase in the charge mobility. The charge mobility of 3.2×10^{-1} $cm^2V^{-1}s^{-1}$ found for the annealed Pt(OX) film-based transistor is the highest value reported for an OTFT fabricated from a porphyrin or metalloporphyrin. This charge mobility is higher than the values (0.01–0.1 $cm^2V^{-1}s^{-1}$) found for the OTFTs constructed from the Pt-containing chain complex $[Pt(NH_2dmoc)_4][PtCl_4]_\infty$ [NH_2dmoc = (*S*)-1-amino-3,7-dimethyloctane],[27] α-ω-dialky-oligothiophenes,[28a–c] and poly(3-hexylthiophene).[28d]

As the majority of as-deposited and annealed thin films studied in this work were crystalline, with one or two strong diffraction peak(s) at 2θ values of 6.73–9.32°, the long axis of the porphyrin molecule is found to be preferentially oriented along one direction with the *d* spacing value at around 9.51–13.14 Å. This suggestion is consistent with the packing of molecules found in the X-ray crystal structures of Pt(Por) complexes (H_2Por = H_2OX, H_2OEP, H_2TBP, H_2Pc, and H_2TPrPc). Based on a chosen Miller plane of the X-ray crystal structure and the observed molecular orientation in the X-ray crystal structure, we propose that the molecular orientation angle ϕ of Pt(Por) in a thin film could be evaluated from an approximate molecular size of Pt(Por) and *d* spacing value of the observed GIXRD peak. The ϕ angles for thin films containing other porphyrin macrocycles are listed in the Supporting information, Table S4.

For the as-deposited Pt(OX) film, the two molecular orientation angles ϕ were 53.7° and 46.9°, which decreased to 40.3° after an annealing treatment at 80 °C. This annealing treatment led to a remarkable increase in the charge mobility of the bottom-contact Pt(OX) field-effect transistor by 10^4-fold. Among the Pt^{II} complexes studied in this work, the unique spatial arrangement of the methyl and ethyl substituents of Pt(OX) accounts for the formation of a spatially-optimized pseudo-2D packing arrangement of Pt(OX) molecules with extensive lateral aggregations and weak π···π stacking interactions. As a result, the charge carrier can readily move in two dimensions along the Pt(OX) film, which may account for the high charge mobility of 3.2×10^{-1} $cm^2V^{-1}s^{-1}$. In the literature, a π-conjugated organic polymer, poly(3-hexylthiophene) with a high charge mobility of 0.1 $cm^2V^{-1}s^{-1}$ was studied by in-plane/out-of-plane grazing incidence synchrotron X-ray diffraction. This polymer has a well-ordered lamellar structure with inter-chain stacking interactions.[29] Using the same film deposition conditions and the same annealing treatment, the thin films made from Pt(OEP), Pt(Pc), Pt(TBP), and Pt(TPrPc) individually exhibited a rather modest or low charge mobility. In these as-deposited films, the Pt^{II} complexes individually packed into a columnar π-stacked or herringbone arrangement with

relatively large molecular orientation angles [$\phi = 55.2°$ for Pt(OEP), 85.5° for Pt(Pc), 86.1° for Pt(TBP), and 90° for Pt(TPrPc)] (Supporting Information, Table S4). The slightly greater steric demand of the ethyl substituents of Pt(OEP) leads to the formation of a columnar-like stacked arrangement of Pt(OEP) molecules. However, the columnar π-stacks of Pt(OEP) molecules are laterally segregated from each other, revealing that charge transport would be likely confined along the π···π stacking direction. Replacing the eight pyrrolic substituents with four n-butyl substituents at the *meso*-positions of the porphyrin ligand, significantly increased the spacings between the Pt^{II} molecules. The weak Pt···H–C interactions are crucial to maintain a herringbone packing arrangement of Pt(TBP) molecules, which inevitably disfavors any cofacial π···π stacking interactions, thus, accounting for the low charge mobility of the Pt(TBP) film. When the n-butyl *meso*-substituents are replaced by phenyl groups, as in the case of Pt(TPP), no Pt···H–C interaction between the pyrrolic or phenyl H atoms with Pt atoms has been noted.[25a] We found that the charge mobility of both the as-deposited and annealed Pt(TPP) films were less than $10^{-6}\,cm^2V^{-1}s^{-1}$. Our attempts to make crystalline films containing substituted-porphycene molecules in a single molecular orientation were unsuccessful. We suggest that the coexistence of two molecular orientations in the as-deposited and annealed Pt(TPrPc) films would lead to an inefficient molecular packing and poor film quality, and have a low charge mobility. In the literature, the charge mobility of a pentacene-based thin film transistor was found to be sensitive to phase purity. The charge mobility ($10^{-6}\,cm^2V^{-1}s^{-1}$) of the film with pentacene molecules in two separate phases was found to be significantly lower than that of the film with one phase ($10^{-6}\,cm^2V^{-1}s^{-1}$ vs $10^{-1}\,cm^2V^{-1}s^{-1}$).[30] Apart from π···π stacking interactions, both the film quality and morphological features of pentacene film-based transistors were found to affect the charge mobility.[31]

In a previous study,[8b] a charge mobility of approximately $10^{-4}\,cm^2V^{-1}s^{-1}$ was reported for a Pt(Pc) film OTFT device, which is higher than the value of $1.5\times10^{-6}\,cm^2V^{-1}s^{-1}$ obtained in this work. A possible explanation for this discrepancy is that there may be two crystal polymorphs, namely, monoclinic and triclinic or α- and γ-Pt(Pc) forms,[20b] simultaneously present in the same Pt(Pc) film, and the Pt(Pc) molecules were packed into two similar types of columnar π-stacked arrangements.[20b] Random distribution of crystal grains of the two polymorphic forms of Pt(Pc) introduced an insulating effect within the film, leading to a decrease in charge mobility. In literature, the occurrence of crystal polymorphism for M(OX), M(OEP), M(TBP), or M(TPP) is less common, with the exception of Ni(OEP)[32] and Cu(OEP).[33] Nevertheless, both the Ni(OEP) and Cu(OEP) films studied in this work exhibited a moderate charge mobility.

Although the crystal structures of M(Por) (where M = Pt, Ni, Cu) do not reveal intermolecular M···M interactions, the metal ion plays an important role in the packing of molecules in the as-deposited and annealed films. As was found for Pt(TBP), the weak Pt···H–C interactions direct the Pt(TBP) molecules to adopt a herringbone-like arrangement, precluding the formation of a columnar-stacked molecular arrangement or any other form of close molecular packing. To the best of our knowledge, there has been no report on close M···H–C contacts in the X-ray crystal structures of Pt^{II} porphyrins in the literature. Short non bonded Ni···H–C contacts of 2.65 Å and 2.76 Å are evident in the X-ray crystal structures of nickel(II) substituted octaethyl-β-oxo-porphyrin[34a] and tetra-*n*-pentylporphyrin, respectively.[34b] Conversely, close Pt···H–C contacts are envisioned to be physically impossible for Pt(OX) and Pt(OEP) molecules, as both complexes do not contain any pyrrolic H atoms and the alkyl substituents (alkyl = methyl or ethyl) are spatially too crowded to bring Pt and H atoms of adjacent molecules into close proximity. This explains why Pt(OX) and Pt(OEP) molecules were individually found to pack with relatively long Pt···H distances of 3.46 Å and 3.33 Å, respectively, in polycrystalline solid samples. The C–H···M interactions have not been observed in the X-ray crystal structures of Ni(OEP) and Pd(OEP). In these two cases, the shortest M···H distances (Å) of 2.970 and 3.394 for the triclinic and tetragonal forms of Ni(OEP), respectively,[17,32] and 3.192 for Pd(OEP),[35] are longer than the sum of van der Waals radii of the metal ion and hydrogen atom (Ni···H 2.83 Å and Pd···H 2.85 Å).[36]

With the exception of M(TPrPc) and M(Pc) (M = Pt and H_2), the charge mobility of the as-deposited and annealed films made from M(OX), M(OEP) (M = Pt, Ni, Cu), or Pt(TBP) were higher than those made from the corresponding metal-free porphyrins. We note that the crystallinity of the films made from M(OX) and M(OEP) (M = Pt, Ni, Cu), and Pt(TBP) were generally better than those made from the respective metal-free porphyrins. The incorporation of a metal ion into the cavity of porphyrin macrocycle increases the rigidity as well as π-conjugation within the porphyrin molecule, and leads to stabilization of X-ray crystal structures by weak intermolecular metal-porphyrin ligand interactions. This generally favors the formation of a robust, well-ordered film structure. For instance, weak Cu···C, Ni···C, or Pt···H interactions are observed in the columnar-like stacked arrangement of Cu(OX) and Ni(OEP) molecules, as well as in the herringbone-like arrangement of Pt(TBP) molecules, respectively. Compared with metal-free porphyrins, the films made from the metalloporphyrins were found to have a higher degree of short- and long-range structural orders, and hence, a higher degree of film crystallinity. Changing the peripheral substituents on Pt^{II} porphyrins readily altered the film morphology arising from the variations in grain size and shape. The degree of film crystallinity and continuity, and concentration of defects and grain boundaries within these thin films altogether affect the charge transport properties. In this work, the formation of a closely-spaced arrangement of Pt(OX) molecules arising from π···π stacking interactions and steric effect of the peripheral methyl and ethyl substituents are probably the most important factors governing the film quality and morphology of the as-depos-

ited Pt(OX) film, leading to excellent overall charge transport properties of the Pt(OX) film-based transistor.

Conclusions

We have constructed a number of field-effect transistors (FETs) made from as-deposited and annealed films of substituted porphyrin compounds and metalloporphyrin complexes, and have measured their charge transport properties. An FET made from an annealed Pt(OX) film exhibited excellent overall charge transport properties, with a charge mobility up to 3.2×10^{-1} $cm^2V^{-1}s^{-1}$. This value is comparable to those of technologically useful organic semiconductors, such as pentacenes and oligothiophenes. The Pt(OX)-based transistor has a charge mobility that is significantly higher than those of analogous metal–organic macrocycles previously reported in literature. The unique molecular shape and peripheral substituents of Pt(OX) enables it to form a robust and efficient molecular packing with extensive lateral aggregations and π···π stacking interactions. This is in contrast to the other Pt^{II} porphyrin complexes that were found to pack into either a columnar π-stacked or herringbone arrangement of the molecules. Annealing treatment of the as-deposited thin film provides a convenient way to maximize the device performance (i.e. charge mobility, on/off ratio, and threshold voltage, etc.), compared with the conventional substrate-heating approach.

Experimental Section

General

All reagents were used as received. The synthetic procedures of M(OX), M(OEP) (where M = Pt, Cu, and Ni), Pt(Pc), H_2(TBP), and the other Pt^{II} complexes studied in this work are given in the Supporting Information. H_2(TPrPc) and Pt(TPrPc) were synthesized according to literature methods.[22c,d] H_2(OX) and H_2(OEP) were purchased from Frontier Scientific and purified by flash column chromatography. ^{1}H NMR spectra were recorded with a Bruker AVANCE 300/400 MHz DRX FT-NMR spectrometers. Electron impact (EI) mass spectra were recorded on a Finnigan MAT 95 mass spectrometer. UV/Vis spectra were recorded on a Perkin–Elmer Lambda 19 UV/Vis spectrophotometer. Elemental analyses were performed at the Institute of Chemistry, Chinese Academy of Science.

Single Crystal X-ray Diffraction

Intensity data for tiny needle-shaped crystals (maximum dimensions <200 μm) of H_2(OX) and Cu(OX), and a thin plate crystal of Pt(OX) were collected using an Oxford Diffraction Kappa diffractometer with enhanced monochromatic CuK_α X-ray radiation ($\lambda=1.54183$ Å) at The Hong Kong University of Science and Technology (HKUST), whereas the X-ray crystal data of Pt(TBP) was recorded using a Maresearch diffractometer equipped with an image plate detector (diameter = 300 mm) using graphite monochromatized MoK_α X-ray radiation ($\lambda=0.71073$ Å) at The University of Hong Kong. For the glass-fiber mounted crystals of Pt(OX), Cu(OX), H_2(OX), and Pt(TBP), the data collection were performed at room temperature. Crystal data and results of structure refinement are given in the Supporting Information, Table S1). All these crystal structures were solved by direct method employing the SHELXS-97 program on a PC.[37] In all cases, the majority of non-H atoms were initially located using Fourier synthesis. Notably, for H_2(OX) and Cu(OX), the lattice constants obtained in this work are different from the reported values determined using powder X-ray data, in which monoclinic cell constants had previously been suggested, but their atomic coordinates are not available in the literature.[38] Nevertheless, the structure solution of H_2(OX) using the space group of *P*-1 failed to achieve a stable convergence (R1 > 20% and R_{wp} ~43%). However, an alternative structure solution using a non centrosymmetric space group (*P*1) gave a model similar to the one solved from the space group *P*-1, and this model was finally refined with a lower R-factor. The two N–H hydrogen atoms were not located in the Fourier difference map. For Pt(OX), owing to the symmetry imposed by the space group $I4_1/amd$ (no. 141 in the International Tables of Crystallography), a half occupancy factor was used for the methyl carbon atom C5 of the ethyl group that was treated as statistically disordered to adopt eight symmetry equivalent sites (x, *y*, *z*; $^1/_4+$y, $^1/_4+$x, $^1/_4-$z; 1−*x*, $^1/_2-$y, z; $^3/_4-$y, $^3/_4-$x, $^1/_4-$z; $^3/_4-$y, $-^1/_4+$x, $^1/_4-$z; 1−*x*, −y, z; $^1/_4+$y, $^3/_4-$x, $^1/_4-$z; x, $^1/_2-$y, z). Structure refinement was performed by full-matrix least-square against F^2 using the SHELXL-97 program.[37] In all these cases, all non-H atoms were refined anisotropically and the aromatic C–H hydrogen atoms were treated as a riding model with isotropic thermal parameters equal to 1.2 times (or 1.5 times for CH_3 and CH_2 moieties) that of the attached C atoms. Crystallographic data (excluding structure factors) for Pt(OX), Cu(OX), H_2(OX), and Pt(TBP) have been deposited in the Cambridge Crystallographic Data Center (CCDC) as supplementary publication numbers: CCDC 642325, 642326, 642327, and 642328. Copies of these data can be obtained free of charge on application to CCDC, 12 Union Road, Cambridge CB2 1EZ, UK (fax: (+44) 1223–336–033; e-mail: deposit@ccdc.cam.ac.uk).

Powder X-ray Diffraction (PXRD)

Solid samples were ground into a fine powder with a mortar and pestle, and were packed onto a glass slide holder. Powder X-ray diffraction patterns were collected with a Bruker D8 Advance (θ/θ) diffractometer equipped with parallel CuK_α radiation ($\lambda=1.5406$ Å) operating at 40 kV and 40 mA. Scan range = 3–60° (2θ), step size = 0.02°, and scan speed = 1 step/second. Prior to any device fabrication, the crystalline-phase purity of the solid samples used in this work was established by comparing the experimental PXRD patterns with the simulated one. Simulated PXRD patterns for M(OX) (M = Pt, Cu, and H_2) and Pt(TBP) were generated using the Mercury 1.4.2 program, that can be downloaded free of charge from the following URL http://www.ccdc.cam.ac.uk/mercury/.

Grazing Incidence X-ray Diffraction (GIXRD)

Grazing incidence X-ray diffraction pattern of as-deposited and annealed films formed on Si/SiO_2 substrate were recorded using a Bruker D8 Advance (θ/θ) diffractometer with a Gobel mirror attachment. Irradiation of the parallel CuK_α X-ray radiation was fixed at a grazing incident angle of 1.000° (θ), and the detector was independently moved to collect the diffraction data in 2θ range of 3–30° with a step-size of 0.01° (2θ) at a fixed speed of 1 step/second.

Field-Effect Transistors and Charge Mobility Measurements

A heavily doped silicon substrate was used as the gate electrode. A silicon dioxide dielectric layer (100 nm) was thermally grown on a silicon substrate. Image reversal photolithography followed by a standard lift-off process was used to form the Ti/Au source/drain contact patterns. The fabricated field-effect transistors had a channel width, *W*, of around 3000–30000 μm and a channel length, *L*, between 6–100 μm. For bottom-contact field-effect transistor, a thin film of metal-free porphyrin or metalloporphyrin with a thickness of 50 nm was coated on the patterned SiO_2/Si substrate by vacuum deposition. For top-contact field-effect transistors ($W=250$ μm and $L=30$ μm), the Au electrode (50 nm) was deposited with a shadow mask under a high vacuum of $<4\times10^{-4}$ Pa, followed by thermal annealing treatment of the metal-free porphyrin or metalloporphyrin film (50 nm) under a high vacuum (10 Pa). The Au electrode was grown at a rate of 0.03 $nm\,s^{-1}$and the sample (porphyrin materials in this work) layer was grown at a rate of 0.3 $nm\,s^{-1}$at room temperature. The output and transfer characteristics of the field-effect transistors were measured inside a N_2 glove box (Mbraun MB20G) equipped with a probe station connected to a semiconductor parameter analyzer (Keith-

ley 4200 SCS). The field-effect charge mobility μ was estimated from the output characteristics in the saturation regime, in which both drain (V_{ds}) and gate (V_g) voltages were −40 V, according to Equation (1):

$$I_{ds} = \frac{W}{2L} C_i \mu (V_g - V_t)^2 \quad (1)$$

(in which, W = channel width; L = channel length; C_i = capacitance of the insulating SiO_2/Si layer; V_g = gate voltage; and V_t = threshold voltage).[39] The device configuration is drawn in Scheme S1 in the Supporting Information.

Thermogravimetric Analysis (TGA)

A few milligrams of solid sample were loaded on an aluminium/platinum crucible. The weight loss of the solid sample was recorded using a Perkin–Elmer TGA-7 analyzer in the temperature range of 30–800 °C under a flowing N_2 stream. The onset decomposition temperatures of all these solid samples are listed in Table 1 and the TGA curves are collectively deposited in the Supporting Information, Figure S8.

Scanning Electron Microscopy (SEM)

Images of film-surface morphology for the field-effect transistors made from the porphyrin materials were recorded using a scanning electron microscopy (LEO 1530). Prior to the SEM image acquisition, all film samples were individually pre-coated with a metallic gold layer with a thickness of 0.5 nm under a high vacuum.

Acknowledgements

This work was supported by the Joint Research Scheme NSFC/RGC (N HKU 742/04); the University Development Fund (Nanotechnology Research Institute, 00600009) of The University of Hong Kong, the Innovation Technology Fund (ITF), Strategic Themes on Nano-Biotechnology and Organic Electronics, University Research Committee of the University of Hong Kong, and RGC of HKSAR (Project No. HKU 7158/04E & HKU 200607176144). We acknowledge Clover & Sunic Systems Ltd. for their support with the fabrication system housed at The University of Hong Kong. SSYC acknowledges the award of postdoctoral fellowship from The University of Hong Kong (HKU). We are grateful to Dr. Herman H. Y. Sung (HKUST) for performing X-ray crystallography on the tiny crystals. We thank Dr. Rory Watt for his kind assistance in proofreading this manuscript.

[1] a) G. Horowitz, *Adv. Mater.* **1998**, *10*, 365; b) H. E. Katz, Z. N. Bao, S. L. Gilat, *Acc. Chem. Res.* **2001**, *34*, 359; c) C. D. Dimitrakopoulos, P. R. L. Malenfant, *Adv. Mater.* **2002**, *14*, 99; d) M. L. Chabinyc, A. Salleo, *Chem. Mater.* **2004**, *16*, 4509.

[2] a) C. D. Dimitrakopoulos, A. R. Brown, A. Pomp, *J. Appl. Phys.* **1996**, *80*, 2501; b) A. Afzali, C. D. Dimitrakopoulos, T. L. Breen, *J. Am. Chem. Soc.* **2002**, *124*, 8812; c) M. M. Payne, S. R. Parkin, J. E. Anthony, C. C. Kuo, T. N. Jackson, *J. Am. Chem. Soc.* **2005**, *127*, 4986.

[3] a) F. Garnier, A. Yassar, R. Hajlaoui, G. Horowitz, F. Deloffre, B. Servet, S. Ries, P. Alnot, *J. Am. Chem. Soc.* **1993**, *115*, 8716; b) A. Facchetti, Y. Deng, A. C. Wang, Y. Koide, H. Sirringhaus, T. J. Marks, R. H. Friend, *Angew. Chem.* **2000**, *112*, 4721; *Angew. Chem. Int. Ed.* **2000**, *39*, 4547; c) A. Facchetti, M. Mushrush, M. H. Yoon, G. R. Hutchison, M. A. Ratner, T. J. Marks, *J. Am. Chem. Soc.* **2004**, *126*, 13859; d) M. H. Yoon, A. Facchetti, C. E. Stern, T. J. Marks, *J. Am. Chem. Soc.* **2006**, *128*, 5792.

[4] V. A. L. Roy, Y. G. Zhi, Z. X. Xu, S. C. Yu, P. W. H. Chan, C. M. Che, *Adv. Mater.* **2005**, *17*, 1258.

[5] Y. L. Wu, Y. N. Li, S. Gardner, B. S. Ong, *J. Am. Chem. Soc.* **2005**, *127*, 614.

[6] Naraso, J.-i. Nishida, S. Ando, J. Yamaguchi, K. Itaka, H. Koinuma, H. Tada, S. Tokito, Y. Yamashita, *J. Am. Chem. Soc.* **2005**, *127*, 10142.

[7] a) G. Horowitz, F. Kouki, P. Spearman, D. Fichou, C. Nogues, X. Pan, F. Garnier, *Adv. Mater.* **1996**, *8*, 242; b) P. R. L. Malenfant, C. D. Dimitrakopoulos, J. D. Gelorme, L. L. Kosbar, T. O. Graham, A. Curioni, W. Andreoni, *Appl. Phys. Lett.* **2002**, *80*, 2517.

[8] a) Z. N. Bao, A. J. Lovinger, A. Dodabalapur, *Appl. Phys. Lett.* **1996**, *69*, 3066; b) Z. N. Bao, A. J. Lovinger, J. Brown, *J. Am. Chem. Soc.* **1998**, *120*, 207; c) W. P. Hu, Y. Q. Liu, S. Q. Zhou, J. Tao, D. F. Xu, D. B. Zhu, *Thin Solid Films* **1999**, *347*, 299; d) K. Xiao, Y. Q. Liu, G. Yu, D. B. Zhu, *Synth. Met.* **2003**, *137*, 991; e) S. I. Noro, H. C. Chang, T. Takenobu, Y. Murayama, T. Kanbara, T. Aoyama, T. Sassa, T. Wada, D. Tanaka, S. Kitagawa, Y. Iwasa, T. Akutagawa, T. Nakamura, *J. Am. Chem. Soc.* **2005**, *127*, 10012; f) Q. X. Tang, H. X. Li, M. He, W. P. Hu, C. M. Liu, K. Q. Chen, C. Wang, Y. Q. Liu, D. B. Zhu, *Adv. Mater.* **2006**, *18*, 65.

[9] a) P. Checcoli, G. Conte, S. Salvatori, R. Paolesse, A. Bolognesi, M. Berliocchi, F. Brunetti, A. D′Amico, A. Di Carlo, P. Lugli, *Synth. Met.* **2003**, *138*, 261; b) S. Aramaki, Y. Sakai, N. Ono, *Appl. Phys. Lett.* **2004**, *84*, 2085; c) P. B. Shea, A. R. Johnson, N. Ono, J. Kanicki, *IEEE Trans. Electron Devices* **2005**, *52*, 1497.

[10] a) Y. Y. Noh, J. J. Kim, K. Yase, S. Nagamatsu, *Appl. Phys. Lett.* **2003**, *83*, 1243; b) Y. Y. Noh, J. J. Kim, Y. Yoshida, K. Yase, *Adv. Mater.* **2003**, *15*, 699.

[11] a) M. A. Baldo, D. F. O'Brien, Y. You, A. Shoustikov, S. Sibley, M. E. Thompson, S. R. Forrest, *Nature* **1998**, *395*, 151; b) R. C. Kwong, S. Sibley, T. Dubovoy, M. Baldo, S. R. Forrest, M. E. Thompson, *Chem. Mater.* **1999**, *11*, 3709; c) H. F. Xiang, S. C. Yu, C. M. Che, P. T. Lai, *Appl. Phys. Lett.* **2003**, *83*, 1518; d) Y. Sun, C. Borek, K. Hanson, P. I. Djurovich, M. E. Thompson, J. Brooks, J. J. Brown, S. R. Forrest, *Appl. Phys. Lett.* **2007**, *90*, 213503.

[12] a) D. B. Papkovsky, G. V. Ponomarev, W. Trettnak, P. O'Leary, *Anal. Chem.* **1995**, *67*, 4112; b) B. H. Han, I. Manners, M. A. Winnik, *Chem. Mater.* **2005**, *17*, 3160.

[13] a) D. B. Papkovsky, T. O'Riordan, A. Soini, *Biochem. Soc. Trans.* **2000**, *28*, 74; b) K. E. Splan, J. T. Hupp, *Langmuir* **2004**, *20*, 10560.

[14] a) Y. Shao, Y. Yang, *Adv. Mater.* **2005**, *17*, 2841; b) A. B. F. Martinson, A. M. Massari, S. J. Lee, R. W. Gurney, K. E. Splan, J. T. Hupp, *J. Electrochem. Soc.* **2006**, *153*, A527.

[15] Z. H. Loh, S. E. Miller, C. J. Chang, S. D. Carpenter, D. G. Nocera, *J. Phys. Chem. A* **2002**, *106*, 11700.

[16] L. R. Milgrom, R. N. Sheppard, A. M. Z. Slawin, D. J. Williams, *Polyhedron* **1988**, *7*, 57.

[17] T. D. Brennan, W. R. Scheidt, J. A. Shelnutt, *J. Am. Chem. Soc.* **1988**, *110*, 3919.

[18] R. Pak, W. R. Scheidt, *Acta Crystallogr. Sect.C* **1991**, *C47*, 431.

[19] J. W. Lauher, J. A. Ibers, *J. Am. Chem. Soc.* **1973**, *95*, 5148.

[20] a) C. J. Brown, *J. Chem. Soc. A* **1968**, 2488; b) C. J. Brown, *J. Chem. Soc. A* **1968**, 2494; c) S. Matsumoto, K. Matsuhama, J. Mizuguchi, *Acta Crystallogr.Sect. C* **1999**, *55*, 131.

[21] M. O. Senge, I. Bischoff, N. Y. Nelson, K. M. Smith, *J. Porphyrins Phthalocyanines* **1999**, *3*, 99.

[22] a) K. M. Smith, *Porphyrins and Metalloporphyrins*, Elsevier, Amsterdam, **1975**; b) A. D. Alder, F. R. Longo, V. Varadi, *Inorg. Synth.* **1976**, *16*, 213; c) E. Vogel, M. Balci, K. Pramod, P. Koch, J. Lex, O. Ermer, *Angew. Chem.* **1987**, *99*, 909; *Angew. Chem. Int. Ed. Engl.* **1987**, *26*, 928; d) C. M. Che, K. K. Cheung, Z. Y. Li, K. Y. Wong, C. C. Wang, Y. Wang, *Polyhedron* **1994**, *13*, 2563; e) K. M. Kadish, K. M. Smith, R. Guilard, *The Porphyrin Handbook*, Academic, San Diego, **2000**.

[23] E. B. Fleischer, *J. Am. Chem. Soc.* **1963**, *85*, 146.

[24] a) D. Braga, F. Grepioni, K. Biradha, G. R. Desiraju, *J. Chem. Soc. Dalton Trans.* **1996**, 3925; b) Y. Zhang, J. C. Lewis, R. G. Bergman, J. A. Ellman, E. Oldfield, *Organometallics* **2006**, *25*, 3515.

[25] a) A. C. Hazell, *Acta Crystallogr. Sect. C* **1984**, *40*, 751; b) H. Furuta, K. Youfu, H. Maeda, A. Osuka, *Angew. Chem.* **2003**, *115*, 2236; *Angew. Chem. Int. Ed.* **2003**, *42*, 2186; c) C. M. Che, Y. J. Hou, M. C. W. Chan, J. H. Guo, Y. Liu, Y. Wang, *J. Mater. Chem.* **2003**,

13, 1362; d) S. W. Lai, Y. J. Hou, C. M. Che, H. L. Pang, K. Y. Wong, C. K. Chang, N. Zhu, *Inorg. Chem.* **2004**, *43*, 3724.

[26] J. Locklin, D. W. Li, S. C. B. Mannsfeld, E. J. Borkent, H. Meng, R. Advincula, Z. N. Bao, *Chem. Mater.* **2005**, *17*, 3366.

[27] W. R. Caseri, H. D. Chanzy, K. Feldman, M. Fontana, P. Smith, A. Tervoort, J. G. P. Goossens, E. W. Meijer, A. P. H. J. Schenning, I. P. Dolbnya, M. G. Debije, M. P. de Haas, J. M. Warman, A. M. van de Craats, R. H. Friend, H. Sirringhaus, N. Stutzmann, *Adv. Mater.* **2003**, *15*, 125.

[28] a) H. E. Katz, J. G. Laquindanum, A. J. Lovinger, *Chem. Mater.* **1998**, *10*, 633; b) J. G. Laquindanum, H. E. Katz, A. J. Lovinger, *J. Am. Chem. Soc.* **1998**, *120*, 664; c) H. Sirringhaus, R. H. Friend, X. C. Li, S. C. Moratti, A. B. Holmes, N. Feeder, *Appl. Phys. Lett.* **1997**, *71*, 3871; d) H. Sirringhaus, N. Tessler, R. H. Friend, *Science* **1998**, *280*, 1741.

[29] H. Sirringhaus, P. J. Brown, R. H. Friend, M. M. Nielsen, K. Bechgaard, B. M. W. Langeveld-Voss, A. J. H. Spiering, R. A. J. Janssen, E. W. Meijer, P. Herwig, D. M. de Leeuw, *Nature* **1999**, *401*, 685.

[30] L. Torsi, A. Dodabalapur, L. J. Rothberg, A. W. P. Fung, H. E. Katz, *Science* **1996**, *272*, 1462.

[31] a) J. G. Laquindanum, H. E. Katz, A. J. Lovinger, A. Dodabalapur, *Chem. Mater.* **1996**, *8*, 2542; b) F. J. Meyer zu Heringdorf, M. C. Reuter, R. M. Tromp, *Nature* **2001**, *412*, 517.

[32] a) E. F. Meyer, Jr., *Acta Crystallogr.Sect. B* **1972**, *28*, 2162; b) D. L. Cullen, E. F. Meyer, *J. Am. Chem. Soc.* **1974**, *96*, 2095.

[33] L. D. Sparks, W. R. Scheidt, J. A. Shelnutt, *Inorg. Chem.* **1992**, *31*, 2191.

[34] a) P. A. Connick, K. J. Haller, K. A. Macor, *Inorg. Chem.* **1993**, *32*, 3256; b) Y. J. Song, R. E. Haddad, S. L. Jia, S. Hok, M. M. Olmstead, D. J. Nurco, N. E. Schore, J. Zhang, J. G. Ma, K. M. Smith, S. Gazeau, J. Pécaut, J. C. Marchon, C. J. Medforth, J. A. Shelnutt, *J. Am. Chem. Soc.* **2005**, *127*, 1179.

[35] A. M. Stolzenberg, L. J. Schussel, J. S. Summers, B. M. Foxman, J. L. Petersen, *Inorg. Chem.* **1992**, *31*, 1678.

[36] a) A. Bondi, *J. Phys. Chem.* **1964**, *68*, 441; b) R. S. Rowland, R. Taylor, *J. Phys. Chem.* **1996**, *100*, 7384.

[37] G. M. Sheldrick, SHELX97 Programs for Crystal Structure Analysis (Release 97–102), University of Göetingen, Germany, **1997**.

[38] a) H. Christ, *Am. Mineral.* **1942**, *27*, 219; b) P. K. Iber, *Anal. Chem.* **1958**, *30*, 2065.

[39] S. M. Sze, *Physics of Semiconductor Devices*, Wiley, New York, **1981**.

Received: January 14, 2008
Published online: June 5, 2008

